Spatial Optimal Interpolation of Aquarius Sea Surface Salinity: Algorithms and Implementation in the North Atlantic

Oleg Melnichenko, Peter Hacker, Nikolai Maximenko, Gary Lagerloef, and James Potemra

Corresponding author: Oleg Melnichenko, Email: oleg@hawaii.edu, Phone: (808) 956-0747. Fax: (808) 956-9425.

ABSTRACT

A method is presented for mapping sea surface salinity (SSS) fields from Aquarius Level 2 along-track data in order to improve the utility of the SSS fields at short length (O ~150 km) and time (O ~1 week) scales. The method is based on optimal interpolation (OI) and provides an SSS estimate at a grid point as a weighted sum of nearby satellite observations. Weights are optimized to minimize the estimation error variance. As an initial demonstration, the method is applied to Aquarius data in the North Atlantic. The key element of the method is that it takes into account the so-called long-wavelength errors (by analogy with altimeter applications), referred to here as inter-beam and ascending/descending biases, that appear to correlate over long distances along the satellite tracks. The proposed method also includes filtering of along-track SSS data prior to OI and the use of realistic correlation scales of mesoscale SSS anomalies. All three features are shown to result in more accurate SSS maps, free from spurious structures. A trial OI SSS analysis is produced in the North Atlantic on a uniform grid with 0.25^{o}-resolution and temporal resolution of one week, encompassing the period from September 2011 through August 2013. A brief statistical description, based on the comparison between SSS maps and concurrent in-situ data, is used to demonstrate the utility of the OI analysis and the potential of Aquarius SSS products to document salinity structure at ~150 km and weekly scales.

1. Introduction.

Sea surface salinity (SSS) is a key parameter that reflects the intensity of the marine hydrological cycle [US CLIVAR Salinity Working Group, 2008]. Aquarius/SAC-D satellite observations provide an opportunity to observe near-global SSS with space and time resolution not available by other components of the Global Ocean Observing System (GOOS).

Aquarius/SAC-D is a collaborative space mission between NASA and Argentina's space agency. Since its launch in June 2011 and onset of data delivery in late August 2011, the Aquarius/SAC-D satellite has been providing space-based observations of SSS with a complete global coverage every 7 days. The satellite is positioned on a polar sun-synchronous orbit crossing the equator at 6 pm (ascending) and 6 am (descending) local time. The Aquarius instrument consists of three microwave radiometers that generate

three beams at different angles relative to the sea surface. The beams form three elliptical footprints on the sea surface (76 x 94 km, 84 x 120 km, and 96 x 156 km) aligned across a ~390-km-wide swath. The emission from the sea surface, measured by the radiometers as an equivalent brightness temperature in Kelvin, is converted to SSS, subject to corrections for various geophysical effects. A detailed description of the Aquarius/SAC-D satellite mission and the Aquarius instrument can be found in: Le Vine et al. [2007]; and Lagerloef et al. [2008].

Since the availability of Aquarius on-orbit data, the calibration/validation team has been actively identifying problems and errors, improving algorithms, and updating the versions of available data. With respect to SSS, significant sources of errors are: temporal sensor drift; ascending/descending biases; and inter-beam biases [Lagerloef et al., 2013]. The latter biases are the focus of the present study. Although there has been steady improvement in the Level 2 SSS versions over the past two years, both the ascending/descending biases and inter-beam biases continue to have significant space-time variability globally, and are the primary source of residual calibration errors in Aquarius SSS retrievals that manifest themselves as artificial north-south striped patterns in mapped SSS fields.
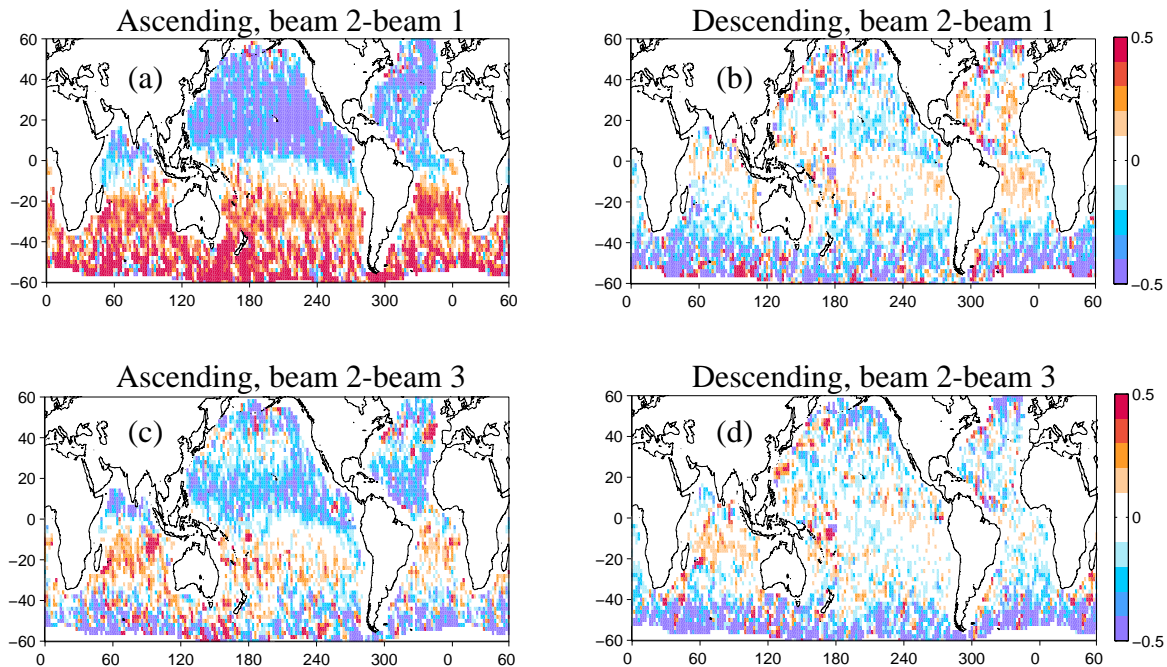

Figure 1. Global maps of inter-beam SSS differences averaged over the month of September 2012. Upper: SSS of beam #2 (middle beam) minus SSS of beam #1 for ascending (a) and descending (b) satellite passes. Lower: SSS of beam #2 minus SSS of beam #3 for ascending (c) and descending (d) satellite passes. Units are psu. Areas where the differences are smaller than 0.2 psu are blanked. The inter-beam SSS differences are computed by differing monthly SSS fields constructed by bin-averaging of raw Aquarius data (each beam separately) within 4° x 4° bins centered on a global grid with the grid spacing of 2° in both zonal and meridional directions.

Figure 1, showing global maps of inter-beam differences averaged over the month of September 2012, illustrates the problem. The differences are shown separately for ascending (from southeast to northwest) and descending (from northeast to southwest) Aquarius passes. In many areas, the inter-beam differences are much larger than 0.2 psu and obviously do not represent the true ocean signal. Note the large-scale structure of the inter-beam differences and the differences between the ascending and descending patterns. The differences also have large amplitude temporal variations with an annual cycle (not shown).

The primary objective of this investigation is to test the possibility of correcting errors in Aquarius SSS data by incorporating available statistical information about the signal and noise into the mapping procedure commonly known as Optimal Interpolation (OI). OI is a fairly straightforward but powerful method of data analysis, extensively used by oceanographers and meteorologists for estimating values of geophysical variables on a regular grid from irregularly sampled observations. The method is based on the Gauss-Markov theorem [Gandin, 1965; Bretherton et al., 1976; McIntosh, 1990] and determines a point-wise estimate of the interpolated field with minimum ensemble mean-square error, given prior information about the variances and correlation functions of the estimated field and the data. The latter requirement is probably the hardest step in practical implementation of the method to the problem of mapping the Aquarius SSS. This is partly due to the fact that in many parts of the ocean there are insufficient high-resolution observations to confidently specify the required statistics of the field [Bingham et al., 2002; Lilly and Lagerloef, 2008]. The attractive feature of OI, however, is that it affords a very convenient way of taking into account error information specific to a given observational platform. This is particularly relevant to the satellite SSS data, since errors in the satellite retrievals are of different types and are spatially correlated [Lagerloef et al., 2013]. Finally, the OI formalism has successfully been applied for mapping various satellite data, such as sea surface temperature [e.g., Reynolds and Smith, 1994; Reynolds et al., 2007; Thiebaux et al., 2003] and sea level anomaly [Le Traon et al., 1998; Ducet et al., 2000]. Many ideas originally developed for these applications are found to be fruitful for the present study as well.

A central goal of the Aquarius satellite mission is to deliver monthly SSS fields at a ~150 km spatial resolution and an accuracy of 0.2 psu [Lagerloef et al. 2008]. In addition to achieving this central goal, we aim to improve the utility (reduce the noise) of the SSS fields at shorter length (O ~ 100 km) and time (O ~ 1 week) scales.

In this paper we focus on the North Atlantic between 0-40°N. The choice of this particular region is motivated by the ongoing field experiment, "Salinity Processes in the Upper-Ocean Regional Study" (SPURS), to study the physical processes that are responsible for the maintenance and magnitude of the subtropical Atlantic salinity maximum. The overall region includes substantial space-time variability of SSS as well as significantly enhanced near-surface, in-situ salinity observations during SPURS.

The rest of the paper is organized as follows. Section 2 provides an overview of the satellite SSS data. Section 3 provides a general description of the algorithm; specifics are

given in Section 4. Section 5 presents results that formally validate the use of the long-wavelength error model to correct Aquarius SSS data for inter-beam biases. An inter-comparison of SSS analyses is presented in Section 6. Section 7 provides the main conclusions and a brief discussion of possible improvements of the analysis.

2. Aquarius SSS data

In the present study, we use Level 2 (L2) version 2.0 Aquarius data produced by the NASA Goddard Space Flight Center's Aquarius Data Processing System (ADPS). The L2 data files, distributed by the Physical Oceanography Distributed Active Archive Center (PO.DAAC) of the Jet Propulsion Laboratory (JPL), contain retrieved SSS, navigation data, ancillary fields, confidence flags, and other related information such as surface winds. The data are structured as a sequence of files, each corresponding to one orbit of Aquarius. An orbit is defined as starting when the satellite passes the South Pole. Individual observations along each orbit consist of a sequence of data points sampled at a 1.44-second (~10 km) interval. Each individual observation represents the average salinity in the upper 1-2 cm layer and over a ~100 km footprint [Le Vine et al., 2007; Lagerloef et al., 2008]. The ancillary SSS data are provided from the global $1/12^o$ data-assimilative Hybrid Coordinate Ocean Model (HYCOM). The model assimilates satellite altimeter observations, satellite and in-situ SST as well as vertical temperature/salinity profiles from Argo floats and moored buoys. In Aquarius L2 data files, the HYCOM SSS is interpolated to the time and location of every Aquarius 1.44-second sample interval.

Figure 2 shows the Aquarius ground tracks over the North Atlantic between the equator and 40^oN. Each track represents three radiometer beams shown by different colors. The Aquarius sampling pattern is quite dense, implying that a variety of commonly used interpolation techniques can be applied to construct a spatially mapped product [Lilly and Lagerloef, 2008]. The problem, however, lies in the relatively large retrieval errors in the satellite SSS data, which, if not corrected, result in spurious structures in the corresponding SSS maps.
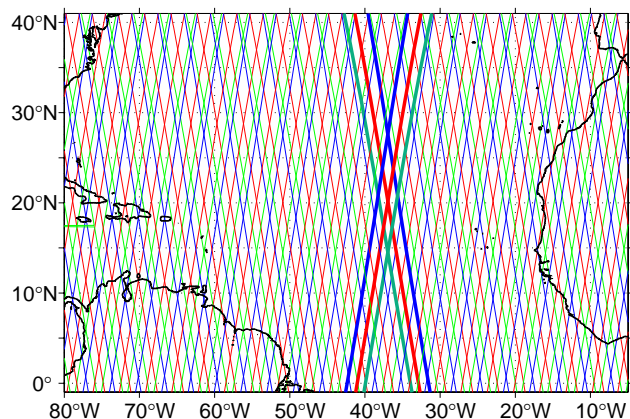

Figure 2. Example pattern of Aquarius ground tracks over the North Atlantic over a 7-day period. Colors indicate the three Aquarius beams. Ascending passes are from south-east to north-west. Heavy lines (green, red and blue) indicate two swaths (ascending and descending) passing through the SPURS domain (38^oW, 25^oN).

4

An example of L2 SSS data is shown in Figure 3, illustrating that there are at least two types of errors in the SSS retrievals. A significant source of error is the accuracy of individual measurements along the satellite tracks. An important aspect of this error is its random character and a very short wavelength. As will be shown later, this short-wavelength noise is essentially 'white' in nature and can effectively be suppressed by averaging over a sufficient number of observations (at the expense of spatial resolution) or by filtering the data along track such as shown in Figure 3 (heavy lines).
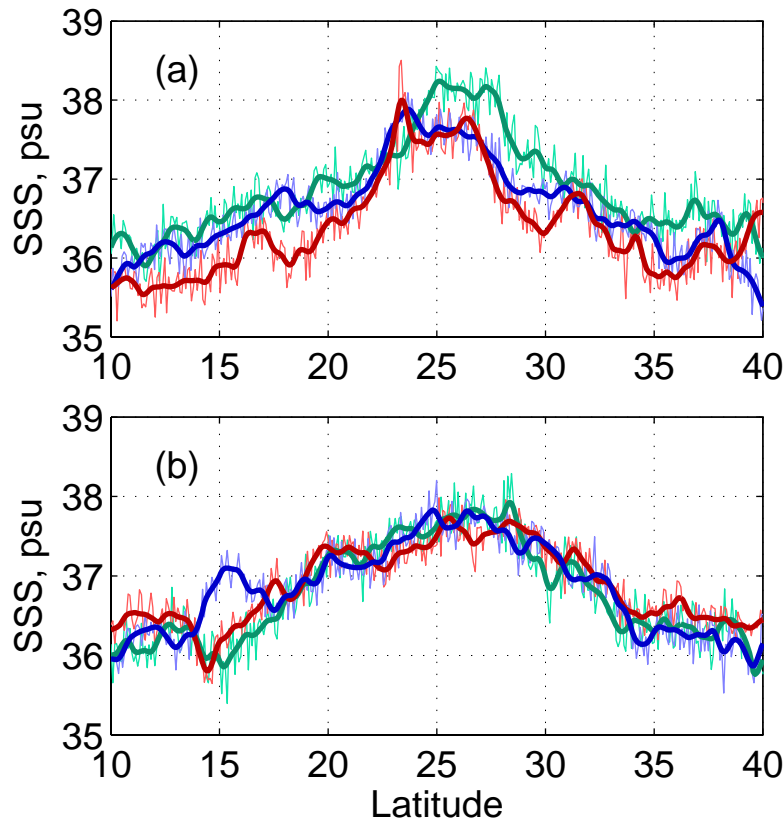

Figure 3. Examples of along-track SSS (3 beams, 390-km wide swath): (a) ascending, passing through the North Atlantic on September 14, 2012, and (b) descending, passing through the North Atlantic on September 11, 2012 (see Figure 2 for locations). Thin curves – raw data; thick curves – smoothed with a running Hanning filter of half-width of ~60 km (approximately half-width of the Aquarius footprint). Colors indicate the three Aquarius beams.

Of much greater concern are differences between the three beams, which can be as large as 0.5-0.8 psu and appear to be correlated over large distances along the satellite tracks. This type of error is also illustrated by Figure 3. During the satellite pass over the North Atlantic on September 14, 2012, the middle beam (red) delivered systematically lower SSS as compared to the other two beams. Such inter-beam biases are likely a manifestation of residual geophysical corrections. Since the three radiometer beams view

the ocean surface at slightly different angles, each beam is affected by geophysical errors differently [Lagerloef et al., 2013].

3. Interpolation procedure

In the interpolation procedure, it is desirable not only to extract all available information from the satellite data, but, simultaneously, correct for various errors. The ultimate goal is to produce the best possible estimate of the evenly gridded SSS field. The OI analysis attempts to accomplish this goal by minimizing the mean square interpolation error for an ensemble of analysis realizations.

3.1. General description of algorithm

The interpolation expression for OI with N observations can be written as [Bretherton et al., 1976; McIntosh, 1990; Le Traon et al., 1998]:

$$\hat{S}_x = S_x^0 + \sum_{i=1}^{N}\sum_{j=1}^{N} A_{ij}^{-1} C_{xj} (S_i^{obs} - S_i^0), \tag{1}$$

where $\hat{S}_x$ is the interpolated value (or estimate) at the grid point $\mathbf{x}$, S_x^0 is the forecast (or "first guess") value at the grid point $\mathbf{x}$, S_i^{obs} is the measured value at the observation point i, S_i^0 is the forecast value at the observation point i, $\mathbf{A}$ is the $N \times N$ covariance matrix of the data

$$A_{ij} = <(S_i^{obs} - S_i^0)(S_j^{obs} - S_j^0)>, \tag{2}$$

and $\mathbf{C}$ is the joint covariance of the data and the field to be estimated

$$C_{xj} = <(S_x - S_x^0)(S_j^{obs} - S_j^0)>. \tag{3}$$

It is generally assumed that the field S_i is imperfectly measured at observation points, yielding values with random errors ε_i : $S_i^{obs} = S_i + \varepsilon_i$. It is also assumed, as is usually reasonable, that the errors and the field are not correlated. Then the general elements of the covariance matrixes (2) and (3) can be written as

$$A_{ij} = <(S_i - S_i^0)(S_j - S_j^0)> + <\varepsilon_i \varepsilon_j>, \tag{4}$$

$$C_{xj} = <(S_x - S_x^0)(S_j - S_j^0)>. \tag{5}$$

6

The analysis is determined relative to the "first guess" field, which is assumed to be a good approximation of the true state. The estimate and the observations are then equal to the "first guess" plus small increments. In this way, the grid point analysis consists of interpolation of the first-guess field to the observation points followed by interpolation of the differences between the observed and first-guess values back to the grid point according to Eq. (1).

The following a priori information is required for construction of a successful OI scheme.

- A background or first guess field with location-dependent values S_x^0, which may be a field of climatological means or continually updated running averages or forecasts [e.g., Clancy et al., 1990; Reynolds and Smith, 1994].
- Covariance of the field to be analyzed. In practice, it is often expressed in a simple analytical form with a few degrees of freedom, allowing for a practical estimation of parameters from observations.
- Covariance of the measurement noise, which can be estimated from an ensemble of realizations of the data, in particular, from a long time-series of the data.

Specific choices of parameters used to construct gridded SSS fields from Aquarius L2 data in the North Atlantic are addresses in the following section.

3.2. Specifics

3.2.1. Preparation of input data.

In order to produce the gridded product, the L2 SSS data are first checked for quality. Data points contaminated by land (land fraction>0.005) are excluded from the analysis. Also excluded from the analysis are data points that are flagged as severely contaminated by radio-frequency interference (RFI), and/or sampled during high wind (wind speed > 15 m/s).

The next step consists of smoothing the along-track SSS data (each beam separately) with a running Hanning filter of half-width of about 60 km to suppress high-frequency instrument noise (e.g. Figure 3). With the Aquarius ~10-km along-track sampling, the filter weighs 12 adjacent observations, which has been found to be quite sufficient to significantly reduce the noise level, yet preserve the ocean signal from over-smoothing.

The effect of filtering of the along-track data is demonstrated in Figure 4, which displays the mean wavenumber spectra of SSS representing the unfiltered and filtered data from the Aquarius repeat track passing through the North Atlantic (see Figure 2 for location). The spectrum of the unfiltered data (blue line) is characterized by a pronounced transition from 'red' to 'white' shape at the wavelength near 100 km. The white spectrum at wavelengths shorter than 100 km is primarily due to the instrument noise. At wavelengths longer than 100 km, the oceanic signal starts to emerge and the power level rises toward the longest wavelength resolved by the spectral analysis. Integrating power of the white noise over the wavenumber domain yields a root-mean-square error of ~0.21 psu. The

signal-to-noise ratio, defined as the ratio of the low-wavenumber signal variance to the high-wavenumber noise variance, is about 40 at 1000-km wavelength and only 10 at 500-km wavelength. After applying the filter procedure (red line) most of the short-wavelength noise is eliminated, while leaving the ocean signal practically unchanged. (This can be shown, for example, by subtracting a flat variance of white noise (0.00025 psu^2) from the blue curve; the result is the green curve). It is likely, however, that residual noise effects are still present in the filtered data, particularly in the form of long-wavelength errors, which are treated separately.
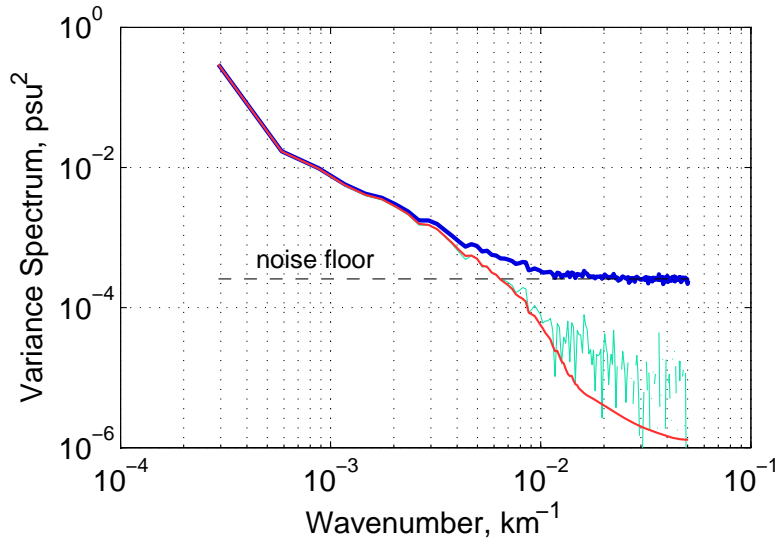

Figure 4. Mean along-track wavenumber spectra of SSS in the area between 10° and 40^oN computed from the data of the ascending portion of the Aquarius repeat swath that passes through the SPURS domain (see Figure 2 for location). The spectra are computed from 73 Aquarius passes (September 2011-April 2013) and the three beams are averaged together. The blue and red curves represent, respectively, the unfiltered and filtered data as described in the text. The total variance associated with the blue and red curves is 0.396 psu^2 and 0.352 psu^2, respectively. The green curve is obtained by subtracting a flat variance of white noise (0.00025 psu^2; black dashed line) from the blue curve.

3.2.2. First guess

The first guess fields, from which deviations are computed by the OI analysis, are derived from monthly mean SSS fields obtained with variational interpolation of Argo buoy measurements. The Argo product is developed at the Asia-Pacific Data-Research Center (APDRC), which provides salinity maps on standard depth levels on a monthly basis (http://apdrc.soest.hawaii.edu/projects/argo/). Figure 5 shows an example of the Argo-derived monthly mean SSS field in the North Atlantic.

The advantage of using Argo-derived SSS fields as the first-guess is two-fold. First, Argo-derived SSS fields are independent of the analysis of the satellite data. Therefore, the data increments, defined as the difference between the data and the first guess, are

8

also independent of the analysis and can be used to compute the error statistics required by OI [Reynolds and Smith, 1994]. Second, Argo-derived SSS fields, since they are based on concurrent data, provide unbiased estimates of the first guess as compared to, say, climatological fields, which can be biased at large-scales due to the presence of significant trends related to climate change [e.g. Durack and Wijffels, 2010] and/or their reliance on highly inhomogeneous multi-type-instrument historical data [Gouretsky and Koltermann, 2007; Wijffels et al., 2008; Roemmich and Gilson, 2009].
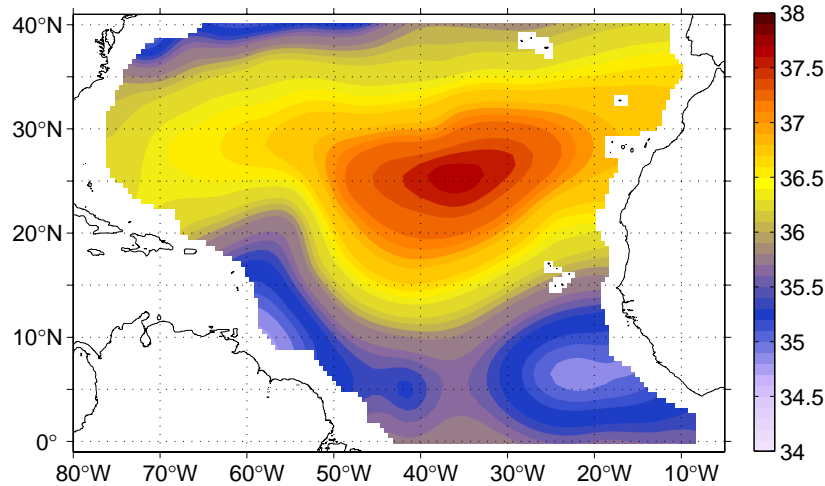

Figure 5. September 2012 mean SSS field from in-situ Argo float data (APDRC product). Units are psu.

3.2.3. Signal statistics

The OI analysis is determined in terms of data increments relative to a first guess. Therefore, the signal statistics, required by OI, must be derived for the data increments relative to the specified first guess [Reynolds and Smith, 1994]. However, the Aquarius along-track data are contaminated by long-wavelength correlated error which may result in correlation functions dominated by these errors. To overcome this problem, the spatial correlation structure of mesoscale SSS anomalies is derived from Aquarius data by dividing the along-track observations into shorter 10°-latitude segments. The basic assumption here is that the dominant wavelengths of the correlated errors are long enough (half-wavelength $> 10^o$ in latitude, Figure 1)) such that the effect of these errors can significantly be reduced by removing liner trends fitted to the along-track SSS data.

The spatial correlation scales of SSS anomalies were computed from Aquarius data as follows. The L2 SSS data (low-pass filtered as described in Sec. 3.2.1) were split into 4 sub-regions, each spanning 10° in latitude: 0-10°N; 10-20°N; 20-30°N; and 30-40°N. The first guess values of SSS were subtracted from the data to obtain the data increments. Here, the first guess values of SSS at observation locations at any given time were obtained by space-time interpolation of the Argo-derived monthly mean SSS fields (Sec.

9

3.2.2). To estimate autocorrelation functions of SSS, linear trends were first removed for each 10° ground-track segment to produce SSS anomalies, presumably free from long-wavelength errors. The along-track autocorrelation functions of SSS anomalies were then estimated for the fractions of ascending and descending paths that span individual 10° sub-regions, assuming that the correlation between two points on a given track is a function only of a distance between the points. Finally, the ensemble mean autocorrelation functions in each sub-region were estimated by averaging over all the corresponding individual autocorrelations.

Figure 6 illustrates the procedure described above. Displayed are ensemble-mean autocorrelations of SSS for the repeat swath shown by the heavy lines in Figure 2. Each color in Figure 6 represents a group of ground-track segments within a particular latitude band. For comparison, autocorrelation functions of ancillary SSS are shown by dashed lines. (The model-derived, L2 ancillary data [Lagerloef et al. 2013] were processed in exactly the same way as Aquarius data (including along-track filtering) except for replacing the first guess by the time-mean over the period of Aquarius observations.) The space-lagged correlations computed from the Aquarius along-track data agree well with the correlations computed from ancillary SSS, providing additional confidence in our approach. Note that ancillary SSS, since it comes from a HYCOM model solution, is free from 'measurement' errors, including long-wavelength errors.
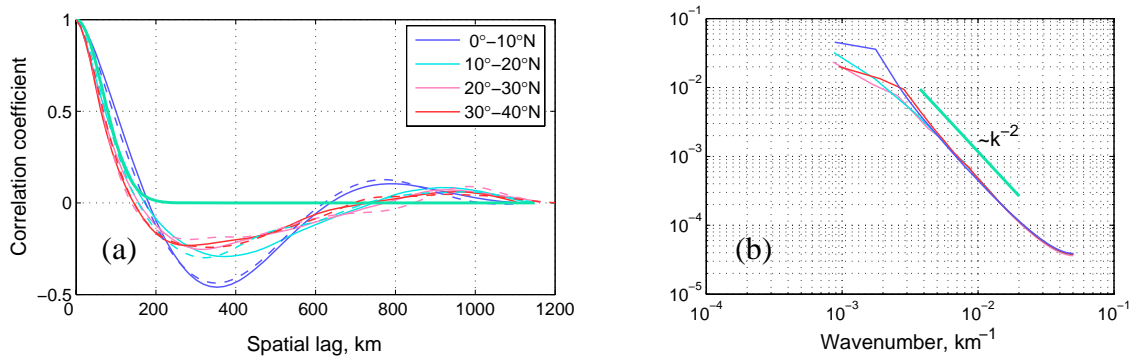

Figure 6. (a) Autocorrelation functions for SSS (solid lines) from the data of the ascending portion of the Aquarius repeat swath that passes through the SPURS domain (see Figure 2 for location). Correlation functions computed from ancillary SSS data are shown by the dashed lines. Different colors correspond to different latitude bands (see text for details). The ensemble-mean approximation by the Gaussian curve is shown by the green line. The corresponding wavenumber spectra (normalized) are shown in (b).

Figure 6 indicates that the structure of the correlation functions is very similar in all latitude bands. The spatial (meridional) scales of mesoscale SSS variability, determined here as the lag of the first zero crossing of the corresponding correlation function, vary little with latitude. They are ~180 km in the zonal band 0-10°N and ~150 km in the zonal band 30-40°N. Because the differences are relatively small, it is reasonable to model SSS variability with a constant spatial decorrelation scale, independent of latitude (see, also,

Table 1). To approximate the observed correlation array, we choose to use a simple Gaussian curve given by

$$c(r) = \exp(-r^2 / R^2) \,, \tag{6}$$

where r is the spatial lag, and $R = 90$ km is the e-folding decay scale.

The Gaussian function with the e-folding scale $R = 90$ km (green curve in Figure 6a) was found to best represent the shape of the ensemble-mean autocorrelation function over the distance range 0-180 km. The corresponding wavenumber spectra are displayed in Figure 6b. In the wavelength range from about 60 km to 300 km, the empirical spectrum follows a power law of the form $\sim k^{-2}$, where k is the wavenumber. Note that the Gaussian-shape autocorrelation function has the decay rate for k that matches that of the observed spectra.

The apparent shortcoming of the Gaussian function, which we select as a statistical model for interpolation of Aquarius SSS, is that it fails to accommodate the negative (oscillatory) lobe of the sample correlation array. Although it is possible, in principle, to utilize a more sophisticated analytical function to fit the estimations, the simpler Gaussian model has been selected for the following reasons. First, one of the strict requirements on the choice of a possible analytical form of the correlation function in the OI analysis is that such a function must be positive definite; that is, the eigenvalues of each resulting correlation matrix must be nonnegative [Gandin, 1965; Bretherton et al., 1976; Thiebaux and Pedder, 1987; Weber and Talkner, 1993]. This is difficult to test for an arbitrary correlation model in two dimensions [Buell, 1972; Weber and Talkner, 1993]. Our experiments with the empirical correlation functions, shown in Figure 6, reveal that their direct use in Eq. (1) may sometimes result in instability of the solution. This is because not all eigenvalues of the corresponding correlation matrixes appear to be positive, which is a necessary condition for a correlation function to correspond to a stationary and homogeneous stochastic process [Yaglom, 1986; Gandin, 1965], assumed in our study. In this regard, the correlation model given by the Gaussian function is proven to be positive definite on every Euclidian space and on the sphere [Yaglom, 1986; Weber and Talkner, 1993], which warrants stability of the algorithm. This choice may not be truly optimal, nonetheless suitable since the decorrelation scales and the major structure of the observed correlations are well reproduced by the Gaussian model (see, also, Appendix). Second, interpolation with the Gaussian function can be considered as a general form of a low pass filter acting on the data [McIntosh, 1990; Sokolov and Rintoul, 1999]. Consideration of the assumptions used to compute correlations from the along-track satellite data suggests that such a low-pass filtration would be more preferable than the case of a band-pass filter, which would correspond to the oscillatory correlation model [Sokolov and Rintoul, 1999]. More sophisticated functional forms could be utilized when more precise data on the SSS correlation structure become available.

The analysis of along-track data gives some useful information about the characteristic meridional scales of SSS variability, but tells us virtually nothing about the zonal scales. One way to overcome this problem is to assume that the spatial correlations are isotropic. This might be true in some areas, but unlikely, for example, in the tropical region where both atmospheric forcing and ocean dynamics are strongly anisotropic [Delcroix et al., 2005; Reverdin et al., 2007]. Yet, limited information exists on the characteristic time and space scales of SSS variability in the ocean [Delcroix et al., 2005; Reverdin et al., 2007]. Studying seasonal variability of SSS in the North Atlantic, Reverdin et al. [2007] find that in most regions outside of the equatorial belt the zonal and meridional scales are comparable, while near the equator the zonal scales are ~1.5-2 times larger than the meridional scales.

To add to the realism of our OI analysis, we also assume that in the tropical region (0-15°N) the zonal scales are larger than the meridional scales and modify Eq. (6) to take an anisotropic form

$$c(r_x, r_y) = \exp(-r_x^2 / R_x^2 - r_y^2 / R_y^2), \qquad (7)$$

where r_x and r_y are spatial lags in the zonal and meridional directions, respectively, and R_x and R_y are the associated zonal and meridional decorrelation scales. The meridional scale is set as R_y=90 km (the same as in the subtropical region), while the zonal scale varies from R_x=180 km at the equator to R_x=90 km at 15°N as follows

$$R_x(y) = 180 \exp(-y^2 / 324), \quad 0^o \le y \le 15^o N, \qquad (8)$$

where y is latitude (in degrees). Near the equator, the aspect ratio R_x / R_y equals 2 (following Reverdin et al. [2007]) and gradually decreases toward higher latitudes. At latitude 15°N, the correlation function (7) becomes isotropic ($R_x = R_y = 90$ km) and matches the correlation function given by (6). We note, however, that our assumptions of the zonal decorrelation scales are somewhat arbitrary due to the lack of appropriate high-resolution SSS data. (It has been determined a posteriori that the use of the anisotropic correlation in the tropics results in slight improvement of the OI SSS analysis).

3.2.4. Error statistics

Analysis of Aquarius along track SSS data (e.g., Figure 3) reveals that there are long-wavelength errors (inter-beam biases) that are correlated over long distances along the satellite tracks. These errors can be as large as 0.5-0.8 psu and manifest themselves as north–south striped patterns in SSS maps constructed by conventional analyses. To incorporate statistical information on these errors into our OI scheme, we adopt the idea that has originally been developed for altimeter applications [e.g., Blanc et al., 1995; Le Traon et al. 1998] and introduce the error covariance model for the Aquarius data in the form

$$< \varepsilon_i \varepsilon_j > = \delta_{ij} \sigma_w^2 + \sigma_L^2 \quad \text{-if data points } i, j \text{ are on the same track and}$$

beam, and in the same cycle, and

$$< \varepsilon_i \varepsilon_j > = \delta_{ij} \sigma_w^2 \qquad \text{-otherwise,}$$

where δ_{ij} is the Kronecker delta, σ_w^2 is the variance of the uncorrelated (white) noise,

and σ_L^2 is the variance of the long-wavelength (along-track) error.

Thus, the algorithm allows two types of random errors to contribute to the elements of the error covariance matrix: the white noise (diagonal elements), representing uncorrelated errors, and the long-wavelength error (off-diagonal elements), representing inter-beam biases that correlate over long distances along the satellite tracks. Each beam is modeled as having independent errors.

Taking into account prior filtering of the along-track SSS, the variance of the white noise in the input data is assumed to be 10% of the signal variance, independent of the geographical location. It is thus assumed that uncorrelated errors, although relatively small, are still present in the data, allowing for some additional smoothing during the OI procedure.

The long-wavelength error in Aquarius observations of SSS is difficult to assess in a direct way due to the lack of a proper reference or "ground truth". To infer the statistical structure of the correlated portion of the retrieval error in Aquarius data, we compare statistics of the inter-beam differences as seen by HYCOM (ancillary SSS) and those evaluated from Aquarius data. In this way, we diminish the effects of large-scale biases that may simultaneously be present in both the Aquarius and HYCOM data.

The statistics of the inter-beam differences are evaluated using Aquarius ground-track segments that span the entire domain from 0° to 40^oN. To eliminate contributions from mesoscale SSS anomalies (Figure 6), the along-track SSS data are low-pass filtered with a running Hanning filter of half-width of ~600 km. The inter-beam differences are computed for each ground-track as SSS of the middle beam (red lines in Figure 2) minus SSS of the two other beams (green and blue lines in Figure 2). The covariances of the inter-beam differences are computed as a function of along-track separation and then averaged over all tracks to obtain the ensemble statistics. The ancillary SSS data are processed in exactly the same way. The estimation of the long-wavelength error statistics is accomplished by comparing the covariances of the inter-beam differences for Aquarius and ancillary SSS.

Figure 7a shows covariances of the inter-beam differences as a function of along-track separation distance for Aquarius (red) and HYCOM (blue) SSS. Notice that the variance of the Aquarius SSS inter-beam differences is consistently larger than its HYCOM counterpart at all lags, presumably due to correlated errors in Aquarius SSS retrievals. Assuming that the inter-beam differences in Aquarius and HYCOM data are not correlated, we can estimate the statistical structure of the long-wavelength retrieval error in Aquarius SSS data as the difference between the Aquarius and HYCOM inter-beam

difference covariances (black). The corresponding variance spectrum is shown in Figure 7b (black).
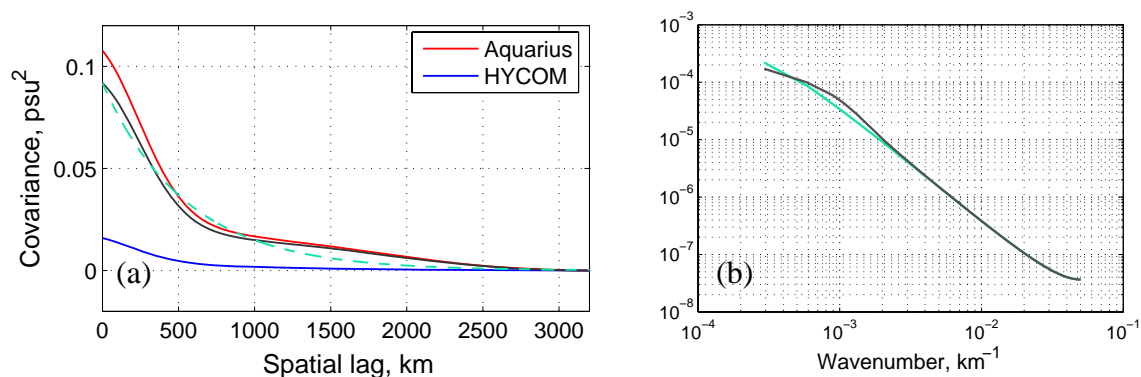

Figure 7. (a) Auto-covariances of inter-beam differences computed from the data of the North Atlantic (0-40°N). Red and blue curves represent Aquarius and ancillary SSS, respectively. The black curve is the difference between the two, representing the covariance of the long-wavelength error in Aquarius data. Its approximation by the exponential function is shown by the green dashed curve. The associated spectra are shown in (b).

Both the covariance function and the spectrum of the long-wavelength error demonstrate that this error has a complex spatial structure. The spectrum is red with more energy concentrated at longer wavelengths with no significant peaks. To obtain a functional form for the long-wavelength error correlation to use in the OI algorithm, we utilize a simple analytical model given by the exponential function of the form

$$C_L(l) = \sigma_L^2 \exp(-l/R_L) , \qquad (9)$$

where l is the along-track separation distance and $R_L = 500$ km is the exponential decay scale. The estimate of R_L is obtained by fitting the curve (9) to the inter-beam bias statistics as shown in Figure 7 by the green curve.

The model (9) is chosen to represent the error correlation structure because this is the simplest model consistent with the data. It provides a good fit to the error correlation array over the distance range 0-600 km over which the correlation is significant, and it satisfies the functional requirements of OI [Webber and Talkner, 1993]

The variance of the long-wavelength error is assumed to be independent of the geographical location ($\sigma_L^2 \approx 0.085$ psu²; Figure 7a, black curve at zero spatial lag). However, the ratio of the error variance to the signal variance is allowed to vary with latitude, following the associated changes in the signal variance (Table 1). These variations are modeled as follows

$$\eta = (1 - \exp(-y^2/225))/1.43 + 0.3, \qquad (10)$$

14

Where η is the long-wavelength error variance to signal variance ratio. Thus, the relative long-wavelength error variance varies from 30% in the near-equatorial region, where the signal variance is large, to 100% at mid-latitudes, where the signal variance is relatively low (Table 1).

3.2.5. Implementation

The OI SSS analysis is computed weekly on a 0.25^o longitude by 0.25^o latitude grid in the North Atlantic between 0°-40°N, covering the period from September 2011 through April 2013. The weeks are defined to correspond to the standard Level 3 product produced by ADPS. The OI SSS analysis is run in a local approximation; namely, only data points in a smaller sub-domain around the analysis grid point are used. The radius of the sub-domain is set to 600 km to accommodate the long-wavelength correlation structure (Figure 6a). This approach seems to be reasonable. Data points beyond this radius contribute very little to the grid-point analysis since the decay length scales for both the signal and error are shorter than 600 km. The local approximation also helps to reduce effects of spatial inhomogeneity in the signal and error statistics [Weber and Talkner, 1993]. Finally, taking into account prior filtering of along track SSS data and to reduce computational load, only one data point out of three (for each track/beam) is retained.

4. Mapping results

The following examples demonstrate the utility of the OI algorithm described above.

Figure 8 compares SSS maps in the North Atlantic for the week August 26 – September 1, 2012 produced by three different analyses, including: (1) standard 7-day Level-3 analysis currently produced by ADPS, (2) conventional OI analysis, hereafter COI, that does not take into account the long-wavelength error ($\sigma_L^2 = 0$), and (3) the advanced OI scheme, hereafter AOI, that takes into account the long-wavelength error as discussed in Section 3.2.4. The standard 7-day Level-3 product is constructed by bin-averaging of Aquarius L2 SSS data within 1°-longitude x 1°-latitude spatial bins centered on a regular 1°-resolution grid. The two OI analyses differ only in the way they treat the long-wavelength error; all other parameters are kept the same.

The bin-average procedure in the standard Level-3 product effectively eliminates high-frequency (white) instrument noise. Yet, it fails to correct for correlated errors (inter-beam biases) which manifest themselves as characteristic north-south striped patterns aligned with the satellite tracks. These stripes are particularly visible when only ascending (Figure 8a) or descending (Figure 8d) data are used as input data to construct the corresponding SSS maps, but also noticeable in the combined data (Figure 8g). The same is true for the COI analysis. While resulting in better spatial resolution, the COI analysis leaves the long-wavelength error untreated such that the satellite tracks appear even more visible in the corresponding SSS maps (Figures 8b, 8e, and 8h). In contrast, the AOI scheme effectively eliminates the along-track correlated errors. The resulting SSS maps constructed from either ascending (Figure 8c) or descending (Figure 8f) data are nearly identical and both resemble the true ocean, free from spurious structures. The

impact of taking into account the long-wavelength error in the OI analysis is further illustrated by comparing the differences between the ascending and descending products (Figures 8 j-l). In the AOI analysis, these differences are significantly reduced.
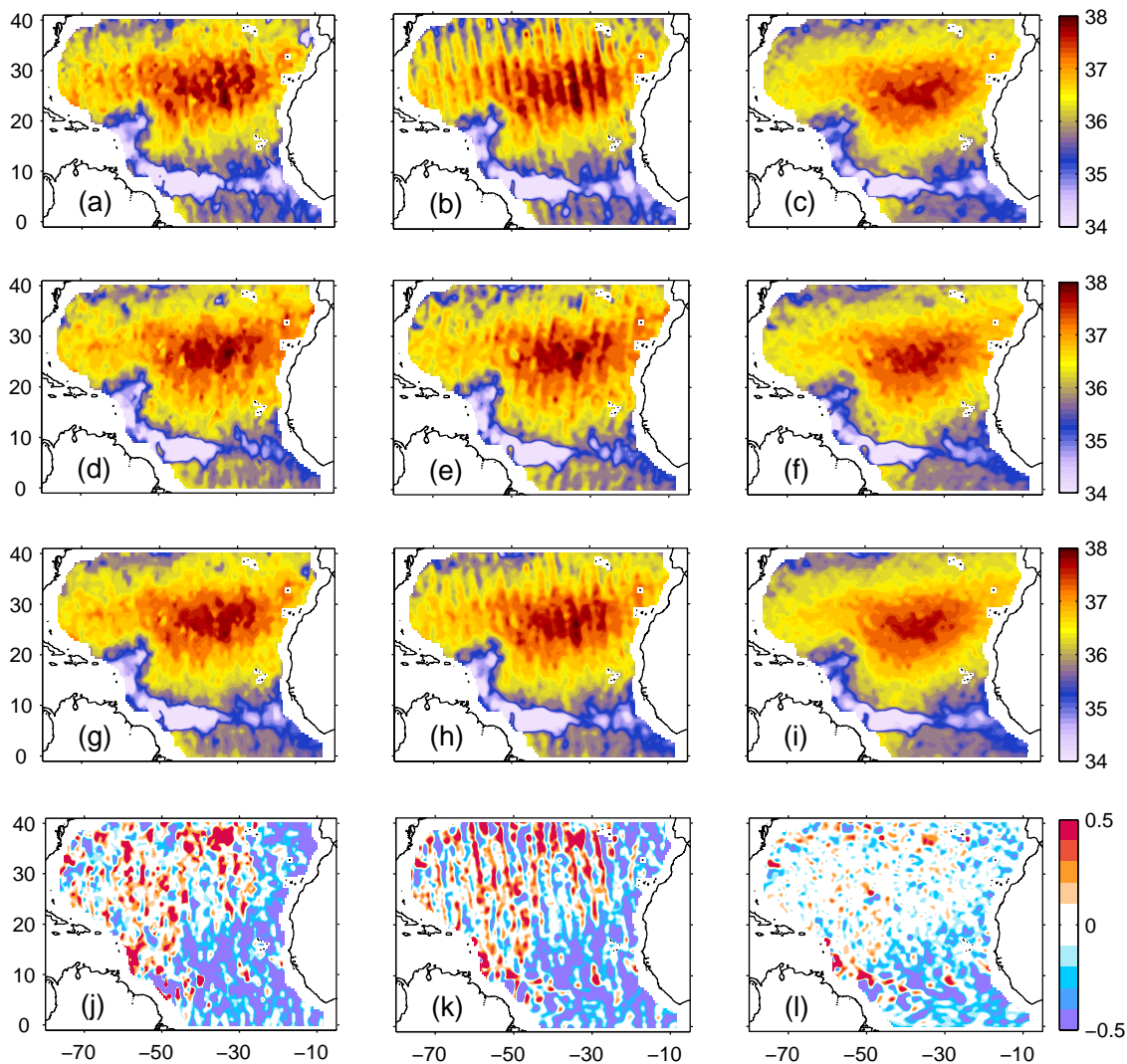

Figure 8. Weekly SSS fields from Aquarius for the week August 27 – September 2, 2012 constructed using different algorithms. Left column: bin-averaging of raw Aquarius L2 SSS data within 1°-longitude x 1°-latitude bins centered on a regular 1°-grid (standard 7-day Level-3 product produced by NASA Goddard; gaps in the maps are filled with linear interpolation. Middle column: conventional OI analysis (COI) that does not take into account the long-wavelength errors (σ_L^2=0). Right column: advanced OI scheme (AOI) that takes into account the long-wavelength error. Upper row (a, b, c) – ascending data; second row (d, e, f) – descending data; third row (g, h, i) – ascending and descending combined; bottom row (j, k, l) – ascending (a, b, c) minus descending (d, e, f), respectively.

The resolution capabilities as well as limitations of the AOI SSS analysis can be inferred from Figure 9, which compares SSS map for the week September 9-15, 2012 with TSG salinity measurements taken from 3-m depth by R/V Thalassa. The in-situ measurements along the ship track reveal numerous small-scale structures with spatial scales smaller than the ~100-km Aquarius footprint. Not surprising, this structures are not resolved in the satellite-derived SSS map. At the same time, it is evident that the analysis is capable of capturing features at scales of at least 150 km. An example is the tongue of low SSS at ~32-33°N followed by the tongue of high SSS to the north (Figure 9b). Unlike the TSG line, the SSS map from Aquarius provides a detailed two-dimensional view on the spatial structure of SSS variability in the region.
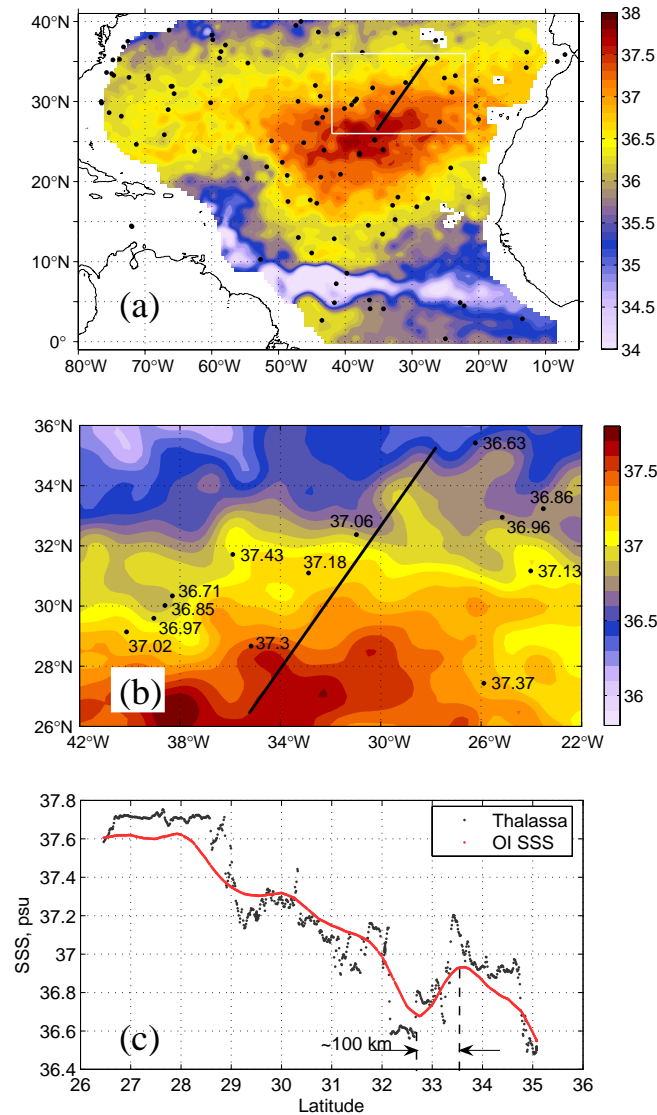

Figure 9. (a) Aquarius OI SSS [psu] for the week September 9-15, 2012. Dots show locations of Argo profiling floats surfaced during the same week. The black line shows locations of TSG measurements taken by R/V Thalassa. (b) The same as in (a) but zoomed in the region 42-22°W, 26-36°N. Note that the color scales in (a) and (b) are different. (c) Comparison of OI SSS map with TSG salinity measurements. The RMSD = 0.12 psu.

The high spatial resolution of weekly OI SSS analyses is further illustrated by Figure 10, which shows example maps of AOI SSS in the tropical North Atlantic for three weeks in July, September, and October 2012. Among the many features represented in Figure 10 is the plume of low salinity water that extends far offshore off the coast of South America. The plume is associated with the Amazon River outflow and is present seasonally during summer and fall and weakens or disappears in other months [Muller-Karger et al., 1988; Lentz, 1995; Ffield, 2006]. The Aquarius SSS maps show a very detailed structure of the plume [Lagerloef, 2012]. Figure 10a shows how the plume starts to spread eastward into the North Atlantic in July 2012, presumably in the retroflection of the North Brazil Current [Muller-Karger et al., 1988; Lentz, 1995]. Over time, as the plume extends farther eastward, it becomes less continuous. However, the boundaries of the plume remain well defined and are characterized by strong SSS gradients.
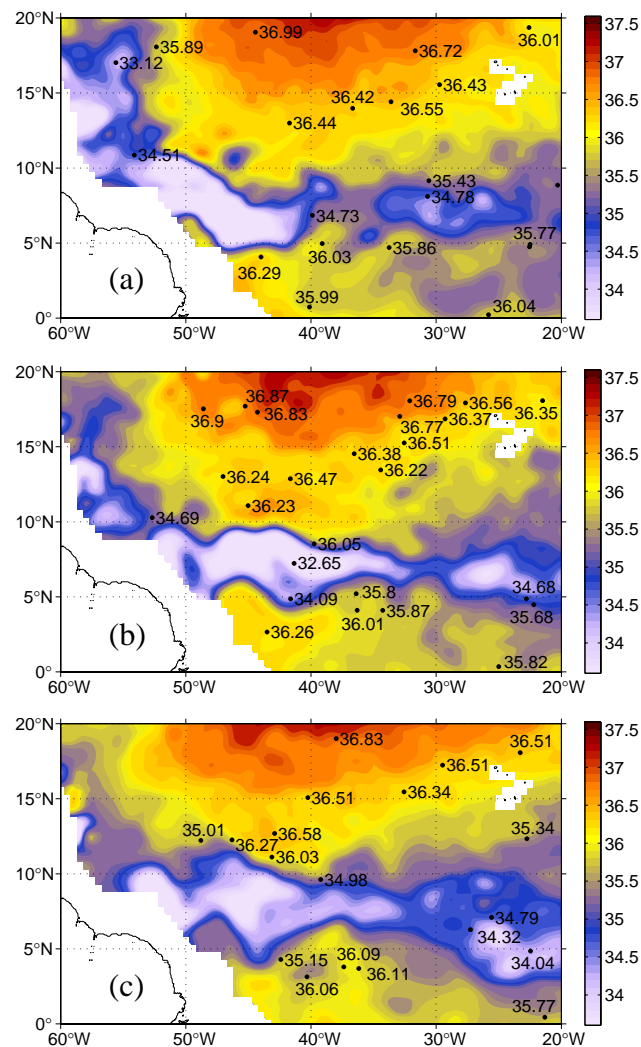

Figure 10. Aquarius OI SSS in the tropical North Atlantic for (a) July 29 – August 4, 2012; (b) September 9-15, 2012; and (c) October 21-27, 2012. Black dots show locations of Argo buoy measurements for the corresponding week.

Finally, to characterize SSS variability in the North Atlantic in one concise picture, Figure 11 shows a time-latitude plot of SSS along the meridional section passing through the SPURS domain. The section coincides with the Aquarius track passing through the SPURS domain (heavy red line in Figure 2). SSS values along the section are obtained by linear interpolation of weekly AOI SSS maps. The analysis demonstrates a consistent pattern of seasonal variability which is most pronounced in the tropical region. A narrow belt of low SSS, presumably associated with the inter-tropical convergence zone (ITCZ), migrates from the southernmost position near the equator in early spring to the northernmost position at about 8^oN in winter. This structure also exhibits rapid temporal changes in some cases and is characterized by strong spatial gradients (see, also, Figure 10). The weakest seasonal variability is observed in the subtropics, particularly in the area of the subtropical salinity maximum. The location of the salinity maximum slightly changes during the course of the year from ~26^oN in fall-winter, when SSS also reaches its maximum, to ~24^oN in late spring, generally consistent with the analysis of historical data (A. Gordon, 2013, personal communication).
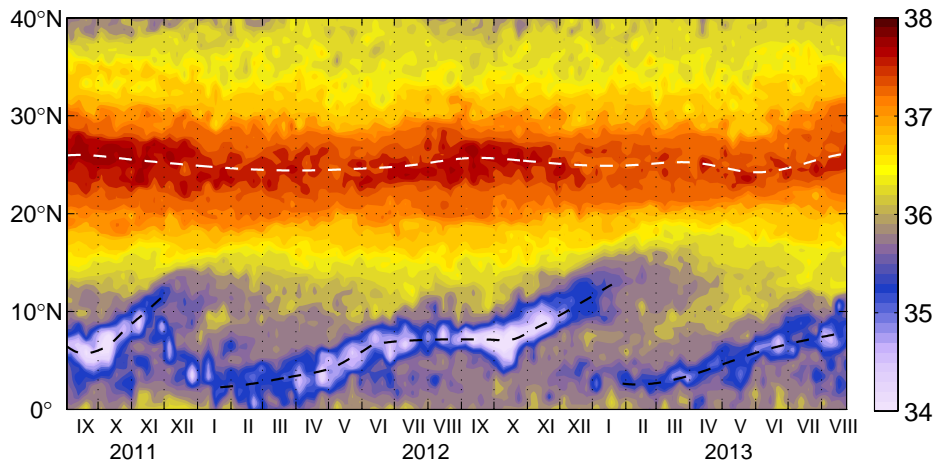

Figure 11. Time-latitude plot of AOI SSS along the meridional section passing through the SPURS domain (the location of section is shown by the heavy red line in Fig. 1). Units are psu. The white dashed line approximates the location of the subtropical SSS maximum. The black dashed line approximates the seasonal march of the Inter-Tropical Convergence Zone (ITCZ).

5. Verification statistics and inter-comparison of SSS analyses

Argo buoy salinity measurements in the near-surface layer are used to provide OI error statistics during the period from September 2011 through August 2013. The error statistics are calculated by comparing buoy measurements for a given week with SSS values at the same locations obtained by interpolating the corresponding Aquarius OI SSS maps. To quantify specifically the effect of incorporating error statistics into the OI algorithm, two versions of the OI analysis are run: one takes into account statistical information on along-track correlated errors (AOI) and the other is the conventional OI algorithm (COI). Also, in order to answer the question whether or not the OI analysis

significantly improves the accuracy of Aquarius-derived SSS maps, the analysis-to-buoy comparisons are made for the standard Level 3 SSS product currently produced by the Goddard Space Flight Center.

The number of buoy data per each week in the North Atlantic is around 80 with quasi-random geographical distribution (e.g., Figure 9a) and remains around this number during the course of Aquarius measurements. The only exception is fall 2012 when a large number of Argo floats were deployed in the SPURS domain. The buoy data are typically drawn at 4-5 m depth and in most cases provide quite accurate representation of SSS. Under certain meteorological conditions, however, the difference between salinity at 5 m depth and the sea surface can be significant and exceed 0.1 psu [Henocq et al., 2010; Melnichenko et al., 2010; Lagerloef et al., 2013].
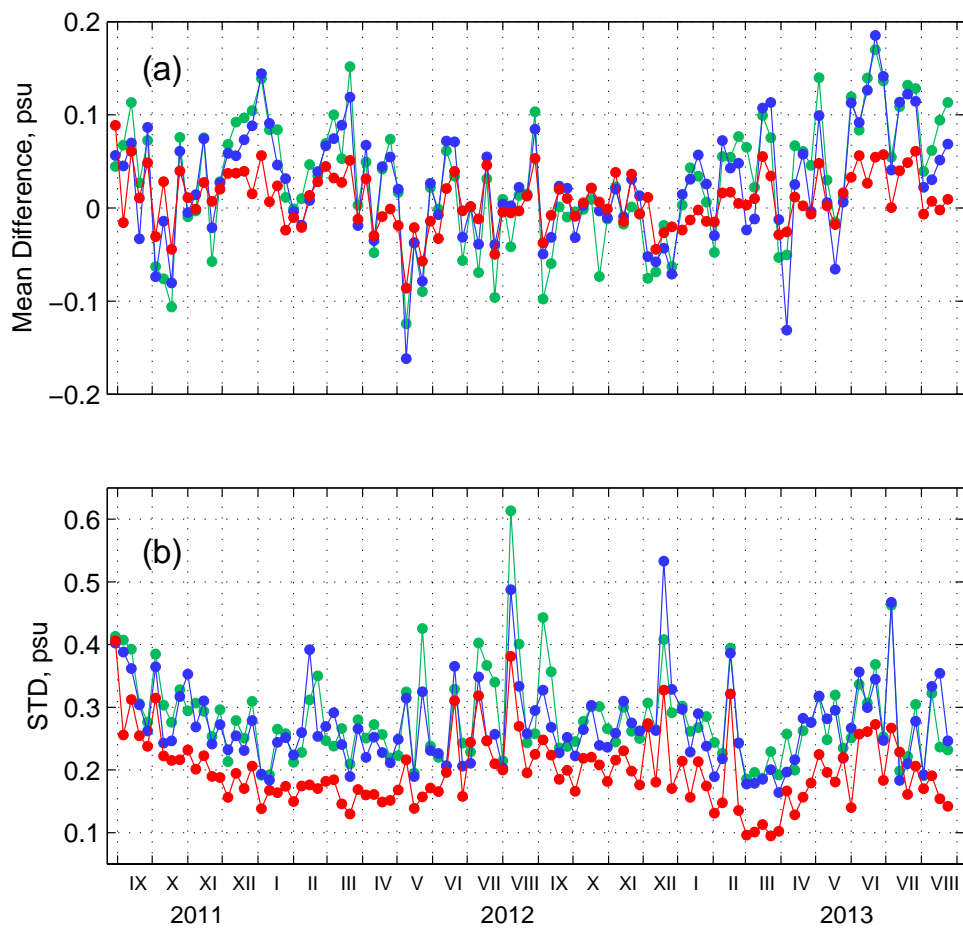

Figure 12. (a) Weekly mean differences and (b) root-mean-square differences between Argo buoy data in the North Atlantic (0-40°N) and three Aquarius SSS analyses: AOI (red), COI (blue); and Level 3 SSS product produced by NASA Goddard (green). The error statistics are computed by comparing Argo buoy measurements for a given week with SSS values at the same locations obtained by interpolation of the corresponding SSS maps.

Figure 12 compares different SSS analyses using common statistics. The mean average of the differences between each product and buoy data over all buoy locations, shown in Figure 12a, is a measure of bias. A negative number in this case implies that on average the SSS estimate from Aquarius data is fresher than the Argo buoy data, and vise versa. The weekly time series of the root-mean-square differences (RMSD) between each of the analyses and buoy data are shown in Figure 12b. Table 2 summarizes the mean, standard deviation, and RMSD of the differences between the analyses and buoy data for the 104-week period of comparison.

Several conclusions can be made from Figure 12 and Table 2. First, the average biases for the three analyses are all smaller than 0.03 psu. However, the weekly time series of the biases (Figure 12a) reveal that there are periods, such as in the fall of 2011, when the biases are significant. For example, the COI analysis and the standard Level 3 product are both ~0.08 psu fresher than the buoy data in October 2011 and ~0.1 psu saltier than the buoy data in January 2012. The AOI analysis results in much smaller biases, but does not completely eliminate them. All three analyses exhibit periods of both negative and positive biases that tend to cancel each other over the 104-week period of comparison. In general, the standard deviation of the weekly biases is the smallest for the AOI analysis as compared to the other two analyses (Table 2).

The RMSD differ significantly for the three analyses. On average, the RMSD of the AOI analysis is about 35% less than that of the COI analysis and about 40% less than that of the standard Level 3 product (Table 2). Figure 12b demonstrates that the AOI analysis has the lowest RMSD with respect to the buoy data for nearly all weeks. In all three analyses, the buoy-to-analysis comparison has the worst RMSD in spring and summer. This is likely a reflection of the fact that very shallow mixed layers are often formed in spring and summer so that salinity at 4-5 m depth measured by a typical Argo buoy may differ from that at the sea surface. A detailed comparison (not shown here) indicates that multiple spikes in the RMSD time series, particularly in the standard Level 3 product, are caused by a few buoys located in the tropics. The fact that the spikes are observed in spring and summer suggests that these spikes are likely due to misrepresentation of SSS by the Argo buoy measurements, as discussed above. It is also important to note that the RMSD of the AOI analysis is smaller than 0.2 for nearly all weeks during the winter season when, due to surface cooling and usually stronger winds, mixing penetrates to greater depths; thus, buoy measurements at 4-5 m depth provide more accurate representation of SSS.

The utility of the AOI product is further illustrated by Figure 13, which compares histograms of the differences between the buoy data in the North Atlantic (0-40°N) and the three SSS analyses. The AOI estimates have an overall good agreement with the buoy data such that the histogram of the differences is quite narrow, with ~55% of the differences falling into the range [-0.1, 0.1] psu. For comparison, this number is 36% for the COI analysis and about 34% for the standard Level 3 product. The number of outliers, defined here as the differences larger than 0.5 psu, is about 3% in the AOI analysis, 5% in the COI analysis, and 6% in the standard Level 3 product. One should keep in mind, however, that the relatively poor performance of the standard Level 3 product with

respect to the buoy data is partly due to the coarser grid on which the product is constructed.
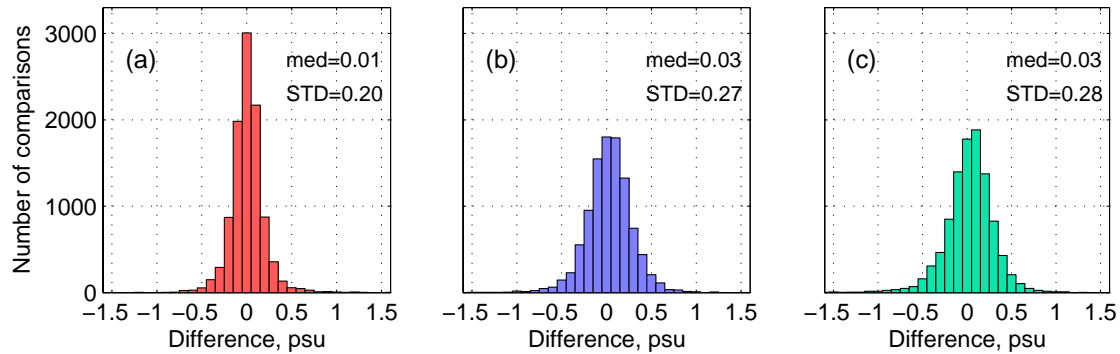

Figure 13. Statistics of the differences between Argo buoy data in the North Atlantic (0-40°N) and three Aquarius SSS analyses: (a) AOI; (b) COI; and (c) Level 3 SSS product produced by NASA Goddard. The error statistics are computed by comparing Argo buoy measurements for a given week with SSS values at the same locations obtained by interpolation of the corresponding Aquarius SSS maps.
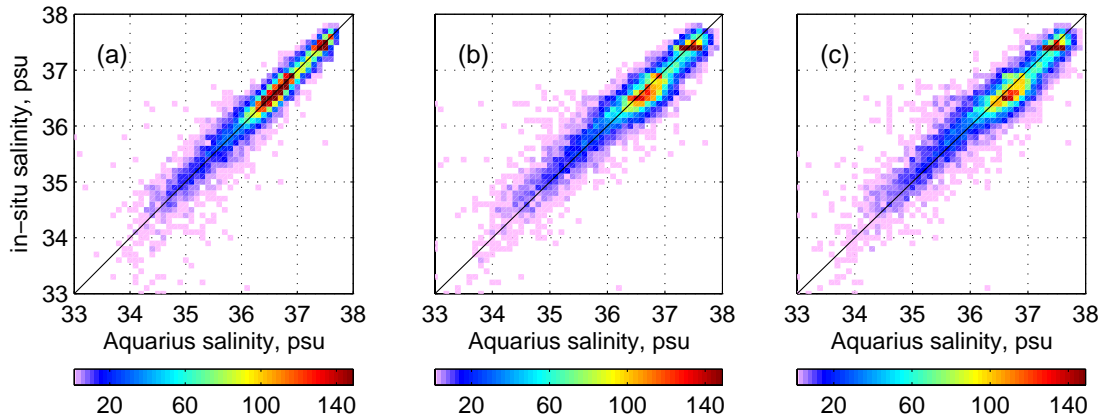

Figure 14. Scatter plots of Aquarius weekly SSS analyses and collocated Argo buoy data in the North Atlantic (0-40°N). The Aquarius SSS analyses are: (a) AOI; (b) COI; and (c) Level 3 SSS product produced by NASA Goddard. Colors represent the number of points in 0.1-psu bins. The error statistics are computed by comparing Argo buoy measurements for a given week with SSS values at the same locations obtained by interpolation of the corresponding Aquarius SSS maps.

Finally, Figure 14 shows the scatter plots between the Aquarius SSS (mapped by the three analyses) and Argo buoy data, which clearly demonstrates where most of the close agreement between the AOI SSS analysis and in-situ data is achieved. The scatter of points is considerably reduced over the regions where SSS is higher than ~35.5 psu (yellow-to-red colors in Figure 5), but remains significant over fresher areas, generally in the tropics (blue-to-magenta colors in Figure 5). There are a few possible explanations for this effect. First, the tropics are characterized by vigorous variability at different space

and time scales (Figure 11), including small-scale variability. In the presence of strong spatial gradients (e.g., Figure 10), the difference between a point measurement by a buoy and the area-averaged SSS sampled by Aquarius can exceed 0.2 psu (Lagerloef et al., 2010). Another source of discrepancy can be related to strong vertical gradients of salinity in the near-surface layer, such that salinity at 5 m depth, sampled by a typical Argo buoy, differs significantly from the surface salinity, sampled by Aquarius. Vertical salinity differences larger than 0.1 psu (sometimes as large as 1.0 psu) are often observed in the tropical belt between the equator and 15°N, which coincides with the average position of ITCZ (Henocq et al., 2010). It follows that the observed relatively large discrepancies between the Aquarius and buoy data in the tropics are not necessarily errors in Aquarius measurements or errors in the mapping procedure, but may rather reflect the disparity between time and space scales captured by two different observational platforms.

6. Summary and discussion

A method has been presented for mapping SSS fields from Aquarius Level 2 data. The method is based on optimal interpolation (OI) and estimates SSS at a grid point as a weighted sum of nearby satellite observations with the weights optimized to minimize the estimation error variance. The key element of the proposed OI algorithm is that it takes into account statistics of correlated errors in the satellite retrievals, referred to here as inter-beam biases that appear to correlate over long distances along the satellite tracks. The inclusion of this type of error information into the OI algorithm has been shown to result in more accurate SSS maps, free from spurious structures.

Examples have been presented that suggest that the OI technique can be an effective tool for mapping Aquarius SSS while correcting for various errors in the data. The quality of the OI analysis has been demonstrated by considering the agreement between synoptic features in the SSS fields and those observed in independent in-situ data, particularly high-resolution TSG data. The OI analysis has been shown to resolve SSS features at scales of ~150 km and larger, consistent with the limited resolution of the input data, and to observe North Atlantic SSS with space and time resolution not available from the present global Argo array.

A trial OI SSS analysis is produced in the North Atlantic (0-40^{0}N) on a uniform grid with 0.25^o grid resolution and with a temporal resolution of one week. Statistical comparison of the OI analysis with respect to the Argo buoy data demonstrates its superior performance as compared to the standard Level 3 product currently produced by the NASA Goddard Space Flight Center's Aquarius Data Processing System (ADPS). In particular, the average root-mean-square error of the OI analysis is ~40% smaller than that of the standard Level 3 product.

It is worth emphasizing that the analysis presented in this paper is to a large extent experimental, focusing on a limited area in the North Atlantic. The results can be considered only 'sub-optimal' in the sense that the signal and error statistics, required by the OI analysis, are determined approximately. Many assumptions have been made, some

of which are not fully justified. In particular, the analysis scheme described here assumes both homogeneity and stationarity of the signal and error statistics, which is certainly one of the weakest aspects of the analysis. This is particularly relevant to the error correlation matrix. The results indicate that incorporating error information into the mapping procedure has dramatic effect on the quality of resulting SSS maps. Seasonal and geographical variations in the variance and/or length scales of the correlated errors in Aquarius SSS retrievals are likely very important factors to consider, but these are beyond the scope of the present paper and will be evaluated in future studies.

Users of Aquarius SSS data should be aware that there are large-scale, space-time varying satellite biases relative to the in-situ data in the present global products [Lagerloef et al., 2013]. This problem seems to be not severe for the North Atlantic between 0-40°N (Figure 12a), but must be addressed in future global and regional analyses. Although the quality of Aquarius L2 data will surely improve in future data versions as processing algorithms improve, the methodology presented in this paper should continue to provide value-added SSS products for regional, high-resolution studies.

Digital data of the weekly OI SSS analysis in the North Atlantic are currently available at http://iprc.soest.hawaii.edu/users/oleg/oisss/atl/ (weekly SSS beginning from September 2011).

Appendix A. Impact of using simplified correlation model in OI SSS analysis.

To examine the effect of using the simplified correlation model for the OI SSS analysis, we computed correlations of SSS anomalies using the data of weekly OI SSS maps. To do this in a straightforward manner, the maps were interpolated into locations of actual observations along the satellite tracks. The SSS correlations were then computed in exactly the same way as using the original L2 data (Section 3.2.3).

Figure A1 illustrates the ensemble-mean autocorrelations of OI SSS for the repeat track shown by the heavy lines in Figure 2. For comparison, autocorrelations computed from

the Aquarius L2 data (Figure 6) are shown by the dashed lines. The figure indicates that the shapes of the space-lagged correlation functions computed from the Aquarius along-track data agree well with those computed from the OI output. This includes not only positive values prior to the first zero-crossings (which are approximated by the Gaussian model) but also the negative lobes at larger lags. The mesoscale SSS variance, however, is much reduced in the OI SSS fields as compared to the along-track data, consistent with the filtering properties of both the signal and error correlation models used in the analysis. The degree of reduction is about 1.5 times in the tropics and up to 3 times at higher latitudes.
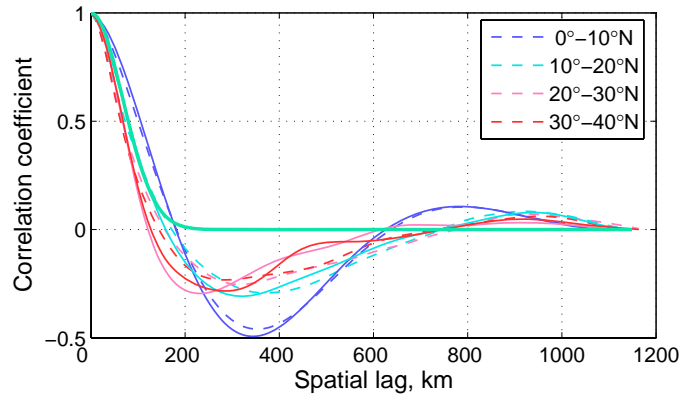

Figure A1. Solid lines show the ensemble-mean autocorrelations of OI SSS for the ascending portion of the Aquarius repeat swath that passes through the SPURS domain (see Figure 2 for location).   Different colors correspond to different latitude bands. To compute these autocorrelations, weekly OI SSS maps were interpolated into locations of actual satellite observations along the satellite track. For comparison, autocorrelations computed from the Aquarius L2 data (Section 3.2.3; Figure 6) are reproduced here by the dashed lines. The green curve is the Gaussian function used in the OI analysis.

Table 1. The variance and correlation length scales (the lag of the first zero crossing of the spatial correlation function) of mesoscale SSS variability as seen by Aquarius in 10-degree latitude bins in the North Atlantic.

Latitude band	Variance, psu^2	Length scale, km
0°-10°N	0.249	150
10°-20°N	0.046	160
20°-30°N	0.023	135
30°-40°N	0.079	140

Table 2. Biases and RMSD statistics between weekly satellite SSS analyses and buoy SSS in the North Atlantic for the period from September 2011 to August 2013.

Analysis	Mean bias, psu	STD of the weekly biases, psu	Mean RMSD, psu
Level 3	0.028	0.065	0.282
COI	0.026	0.06	0.27
AOI	0.009	0.03	0.198

REFERENCES

Bingham, F.M., S.D. Howden, and C.J. Koblinsky, 2002: Sea surface salinity measurements in the historical database, *J. Geophys. Res.*, 107(C12), 8019, doi:10.1029/2000JC000767.

Blanc, F., P.-Y. Le Traon, and S. Houry, 1995: Reducing orbit error with an inverse method to estimate the oceanic variability from satellite altimetry, *J. Atmos. Oceanic Technol.*, 12, 150-160.

Bretherton, F. P., R.E Davis, and C.B. Fandry, 1976: A technique for objective analysis and design of oceanographic experiments applied to MODE-73, *Deep Sea Res.*, 23, 559-582.

Clancy, R.M., P.A. Phoebus, and K.D. Pollak, 1990: An operational global-scale ocean thermal analysis system, *J. Atmos. Oceanic Technol.*, 7, 233-254.

Delcroix, T., M.J. McPhaden, A. Dessier, and Y. Gouriou, 2005: Time and space scales for sea surface salinity in the tropical ocean, *Deep-Sea Res. I*, 52, 787-813.

DiMego, G.J, 1988: The National Meteorological Center regional analysis system, *Mon. Wea. Rev.*, 116, 977-1000.

Ducet, N., P.Y. Le Traon, and G. Reverdin, 2000: Global high-resolution mapping of ocean circulation from TOPEX/Poseidon and ERS-1 and -2, *J. Geophys. Res.*, 105(C8), 19477-18498.

Ffield, A., 2006: Amazon and Orinoco River Plumes and NBC Rings: Bystanders or Participants in Hurricane Events?, *J. Clim.*, 20, 316-333.

Gandin, L.S., 1965: *Objective Analysis of Meteorological Fields*, 242 pp, Israel Program for Scientific Translation, Jerusalem, 1965.

Gouretski, V.V., and K.P. Koltermann, 2007: How much is the ocean really warming? *Geophys. Res. Lett.*, 34, L01610, doi:10.1029/2006GL027834.

Henocq, C., J. Boutin, F. Petitcolin, G. Reverdin, S. Arnault, and P. Lattes, 2010: Vertical variability of Near-Surface Salinity in the Tropics: Consequences for L-Band Radiometer Calibration and Validation, *J. Atmos. Oceanic Technol.*, 27, 192-209.

Lagerloef, G., F.R. Colomb, D. LeVine, F. Wentz, S. Yueh, C. Ruf, J. Lilly, J. Gunn, Y. Chao, A. deCharon, G. Feldman, and C. Swift, 2008: The Aquarius/SAC-D

Mission: Designed to meet the salinity remote-sensing challenge, *Oceanography*, 20(1), 68-81.

Lagerloef, G., 2012: Satellite Mission Monitors Ocean Surface Salinity, *Eos*, 93(25), 233-234.

Lagerloef, G., H.-Y. Kao, O. Melnichenko, P. Hacker, Eric Hackert, Y. Chao, K. Hilburn, T. Meissner, S. Yueh, L. Hong, and T. Lee, 2013: Aquarius salinity Validation Analysis, Aquarius project document AQ-014-PS-0016, JPL, 18 February 2013.

Lentz, S.J., 1995: Seasonal variations in the horizontal structure of the Amazon Plume inferred from historical hydrographic data, *J. Geophys. Res.*, 100(C2), 2391-2400.

Le Vine, D.M., G.S.E. Lagerloef, F.R. Colomb, S.H. Yueh, and F.A. Pellerano, 2007: Aquarius: An instrument to monitor sea surface salinity from Space, *IEEE Transactions on Geoscience and Remote Sensing*, 45(7), 2040-2050.

Lilly, J.M., and G.S.E. Lagerloef, 2008: Aquarius Level 3 processing algorithm: theoretical basis document, Version 0.9, Aquarius Ground Segment, Goddard Space Flight Center.

McIntosh, P.C., 1990: Oceanographic data interpolation: Objective analysis and splines, *J. Geophys. Res.*, 95(C8), 13529-13542.

Melnichenko, O., N.A. Maximenko, J. Potemra, and P. Hacker, 2010: Statistics of near-surface salinity gradients from historical CTD and Argo data, Presentation at the 6th Aquarius/SAC-D Science Meeting, Seattle, Washington, 19-21 July 2010.

Muller-Karger, F.E., C.R. McClain, and P.L. Richardson, 1988: The dispersal of the Amazon's water, *Nature*, 333, 56-58.

Reynolds, R.W., and T.M. Smith, 1994: Improved global sea surface temperature analyses using optimal interpolation, *J. Clim.*, 7, 929-948.

Reynolds, R.W., T.M. Smith, C. Liu, D.B. Chelton, K.S. Casey, and M. Schlax, 2007: Daily High-Resolution-Blended Analyses for Sea Surface Temperature, *J. Clim.*, 20, 5473-5496.

Reynolds, R.W., and D.B. Chelton, 2010: Comparisons of Daily Sea Surface Temperature Analyses for 2007-08, *J. Clim.*, 23, 3545-3562.

Reverdin, G., E. Kestenare, C. Frankignoul, and T. Delcroix, 2007: Surface salinity in the Atlantic Ocean (30°S-50°N), *Prog. Oceanogr.*, 73, 311-340.

Roemmich, D., and J. Gilson, 2009: The 2004-2008 mean and annual cycle of temperature, salinity, and steric height in the global ocean from the Argo program, *Prog. Oceanogr.*, 82, 81-100.

Sokolov, S., and S.R. Rintoul, 1999: Some Remarks on Interpolation of Nonstationary Oceanographic Fields, *J. Atmos. Oceanic Technol.*, 16, 1434-1449.

Thiebaux, H.J., and M.A. Pedder, 1987: *Spatial objective analysis: with applications in atmospheric science*, Academic Press, 299 pp.

Thiebaux, J., E. Rogers, W. Wang, and B. Katz, 2003: A new high-resolution blended real-time global sea surface temperature analysis, *BAMS*, 84, 645-656.

U.S. CLIVAR Office, 2007: Report of the U.S. CLIVAR Salinity Science Working Group, U.S. CLIVAR Report 2007-1, U.S. CLIVAR Office, Washington, DC, 20006, 46 pp.

Weber, R.O., and P. Talkner, 1993: Some Remarks on Spatial Correlation Function Models, *Mon. Wea. Rev.*, 121, 2611-2617.

Wijffels, S.E., J. Willis, C.M. Domingues, P. Barker, N.J. White, A. Gronell, K. Ridgway, and J.A. Church, 2008: Changing expendable bathythermograph fall rates and their impact on estimates of thermosteric sea level rise, *J. Clim.*, 21, 5657-5672.

Yaglom, A.M., 1986: *Correlation Theory of Stationary and Related Random Functions I. Basic Results*, Springer-Verlag, 526 pp.